Self-Supported Ceramic Electrode of 1T-2H MoS_2 grown on TiC Membrane for Hydrogen Production

Yangyang Shi,[†] Dewen Zheng,[‡] Xi Zhang,[‡] Kai Lv,[†] Feihong Wang,[†] Binbin Dong,[†] Shanyu Wang,[‡] Chunxia Yang,[‡] Jianming Li,[‡] Fengyi Yang,[†] Lu Yuan Hao,[†] Liangjun Yin,[§] Xin Xu,[*,†] Yuxi Xian,[*,∥] and Simeon Agathopoulos[⊥]

[†]CAS Key Laboratory of Materials for Energy Conversion, Department of Materials Science and Engineering, University of Science and Technology of China, Hefei, Anhui 230026, P.R. China

[‡]New Energy Research Center, Research Institute of Petroleum Exploration & Development (RIPED), PetroChina, Beijing 100083, P.R. China

[§]School of Energy Science and Engineering, University of Electronic Science and Technology of China, 2006 Xiyuan Road, Chengdu 611731, P.R. China

[∥]CAS Key Laboratory of Mechanical Behaviors and Design of Materials, Department of Modern Mechanics, University of Science and Technology of China, Hefei, Anhui 230026, P.R. China

[⊥] Department of Materials Science and Engineering, University of Ioannina, GR-451 10 Ioannina, Greece

Corresponding Authors:

*E-mail: xuxin@ustc.edu.cn. Tel.: +86-551-63600824. Fax: +86-18655117978 (Xin Xu).

*E-mail: yxxian@ustc.edu.cn (Yuxi Xian).

Analysis and calculations made from the bands of the XPS spectra

Curve fitting was applied in the high-resolution XPS spectra for Mo 3d and S 2p by subtracting the background with consistency from the fitting peaks with optimized parameters (including binding energy, full width at half maximum and area), assisted by NIST XPS database[1] and according to relevant literature. The integrated area between the line of the peak and the background was defined as the peak intensity. The integrated area was calculated by the XPS software after curve fitting. For each element, we selected a peak and we divided the area of that peak, I_i, by the sensitivity factor, S_i, in order to obtain the normalized peak area, I_i/S_i. The equivalent homogenous atomic fraction, X_i, of each element is the ratio of the normalized peak area divided by the sum of all the normalized peak areas (the atomic percent (at. %) is the product of X_i multiplied by 100).[2] The equation can be denoted as:

$$X=\frac{Ip/Sp}{\sum jIj/Sj}$$

In this equation, the sensitivity factors for Mo 3d in 1T-MoS_2 and 2H-MoS_2 are the same. The relative content of 1T phase in the total MoS_2 can be calculated as:

$$X_{(1T\text{-}MoS2)} = I_{1T}/(I_{1T}+I_{2H}).$$

It is worthy of note that the calculation of 1T content from S 2p is a good match with the result obtained for Mo3d. This further manifests the reliability of this method.

Calculation of thermodynamic magnitudes used in the DFT calculations

The hydrogen adsorption energy (ΔE_H) on S atoms was calculated by the equation (S1):

$$\Delta E_H = E_{(Catalyst + H)} - E_{(Catalyst)} - 1/2\ E(H_2)\text{……(S1)}$$

where $E_{(Catalyst +H)}$ is the total energy of the catalyst with one absorbed H atom, $E_{(Catalyst)}$ is the

total energy of the catalyst without absorbed H atoms, and $E(H_2)$ is the energy of hydrogen molecule in gas phase.[3]

The free energy of the adsorbed state can be calculated by the equation (S2):

$$\Delta G_H = \Delta E_H + \Delta E_{ZPE} - T\Delta S_H \ldots\ldots\ldots\ldots \text{(S2)}$$

where ΔE_{ZPE} is the difference in zero point energy between the adsorbed and the gas phase, and ΔS_H is related to the entropy of adsorption of 1/2 H_2. When these two factors were taken into consideration under standard conditions, ΔG_H was calculated as:

$$\Delta G_H = \Delta E_H + 0.24 \text{ eV} \ldots\ldots\ldots\ldots \text{(S3)}$$

Thus, the free energy of H adsorption for TiC, 2H-MoS_2, 1T-MoS_2, 2H-MoS_2/TiC, and 1T-MoS_2/TiC was calculated.

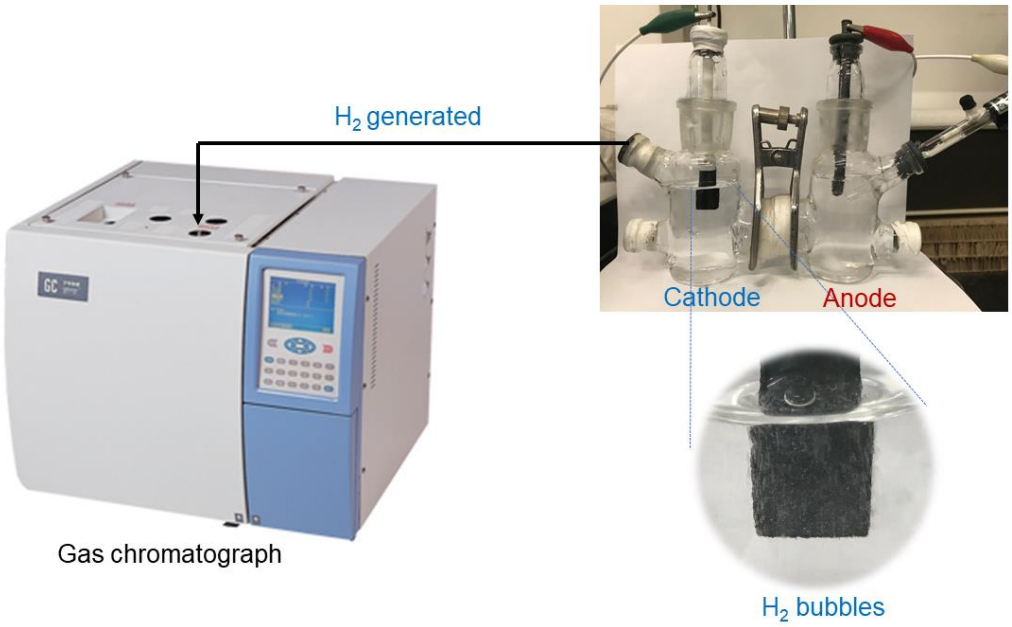

Figure S1. The setup for determining the Faradaic efficiency and the magnification of surface area of the TCMS electrodes.

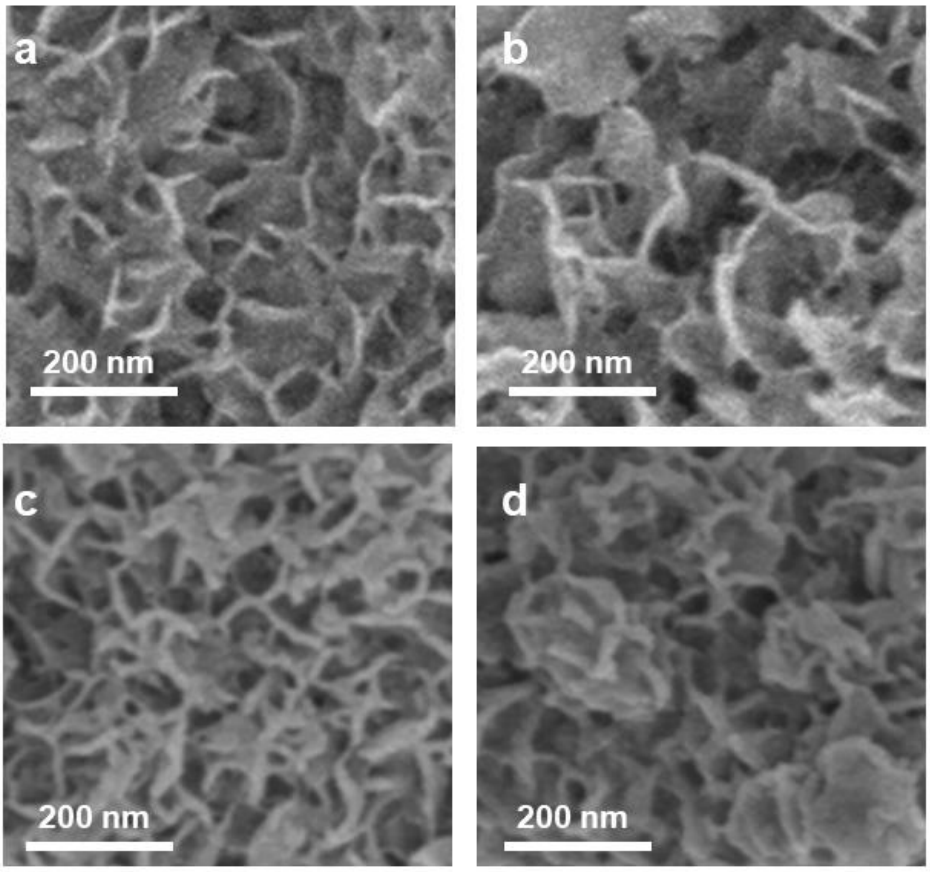

Figure S2. Microstructure of (a) TCMS 1, (b) TCMS 2, (c) TCMS 3, and (d) TCMS 5.

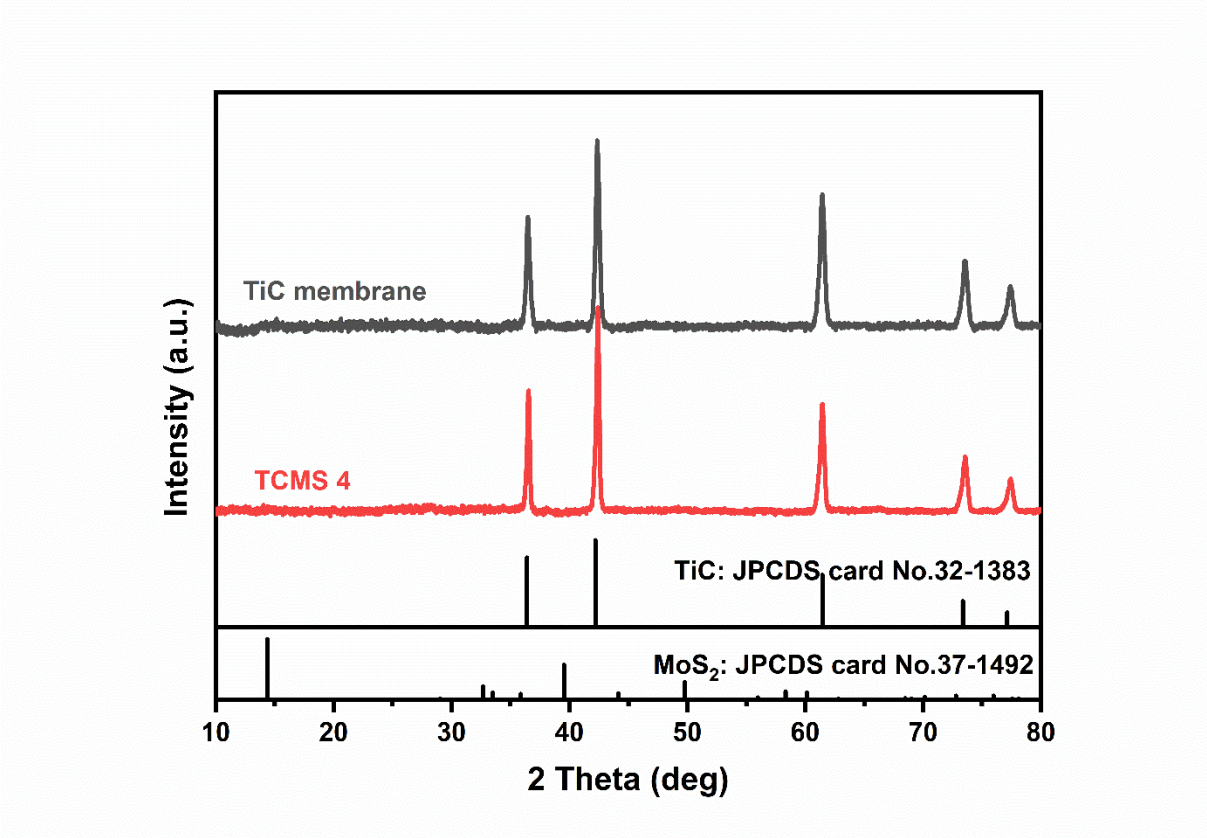

Figure S3. X-ray diffractograms of TiC membrane and TCMS 4.

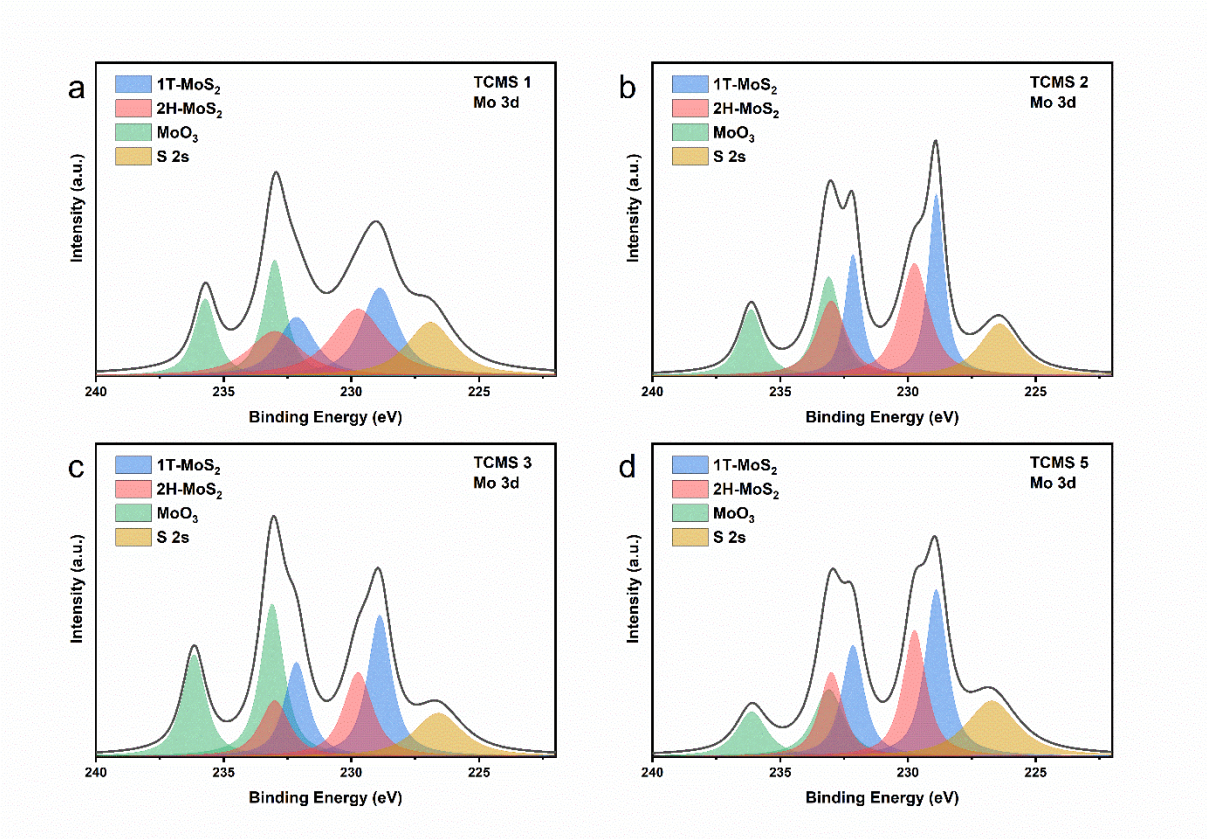

Figure S4. High-resolution XPS spectra of the Mo 3d peak region of (a) TCMS 1, (b) TCMS 2, (c) TCMS 3, and (d) TCMS 5.

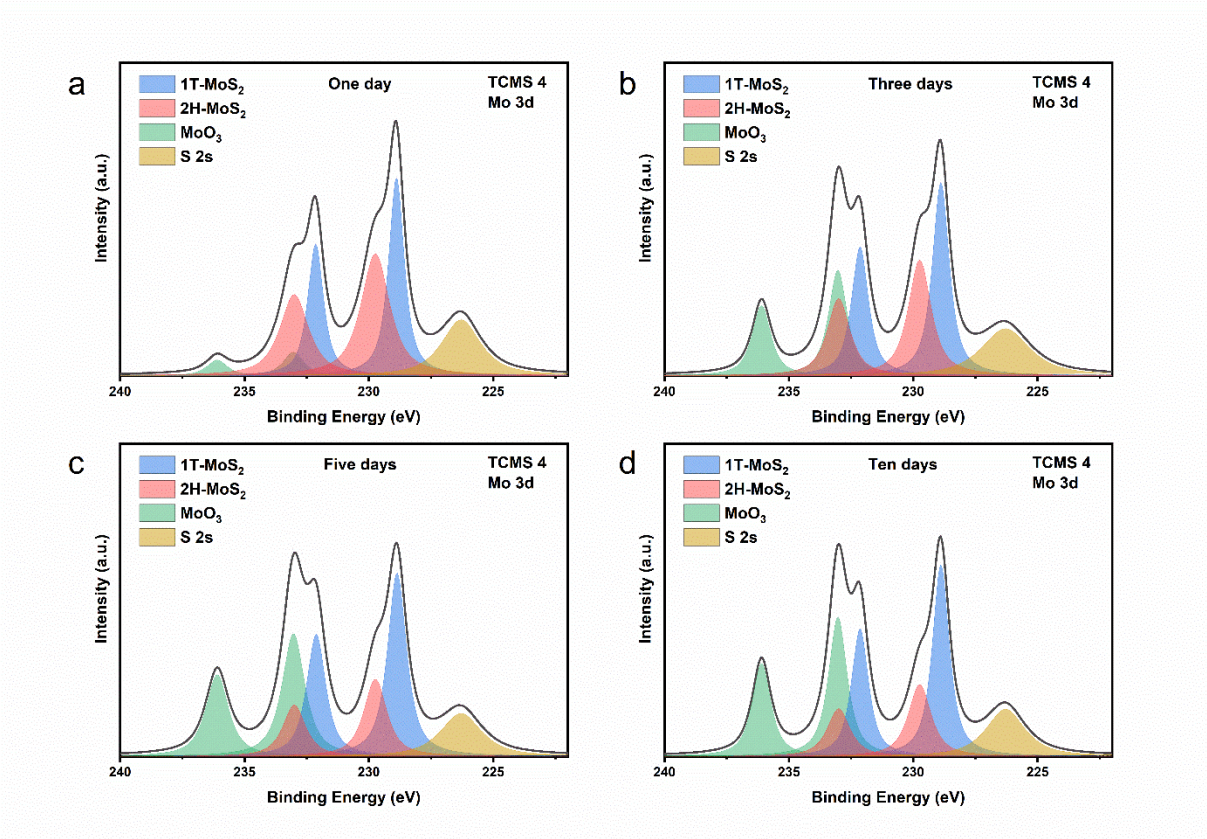

Figure S5. High-resolution XPS spectra of Mo 3d region of TCMS 4 recorded (a) one, (b) three, (c) five, and (d) ten days after preparation.

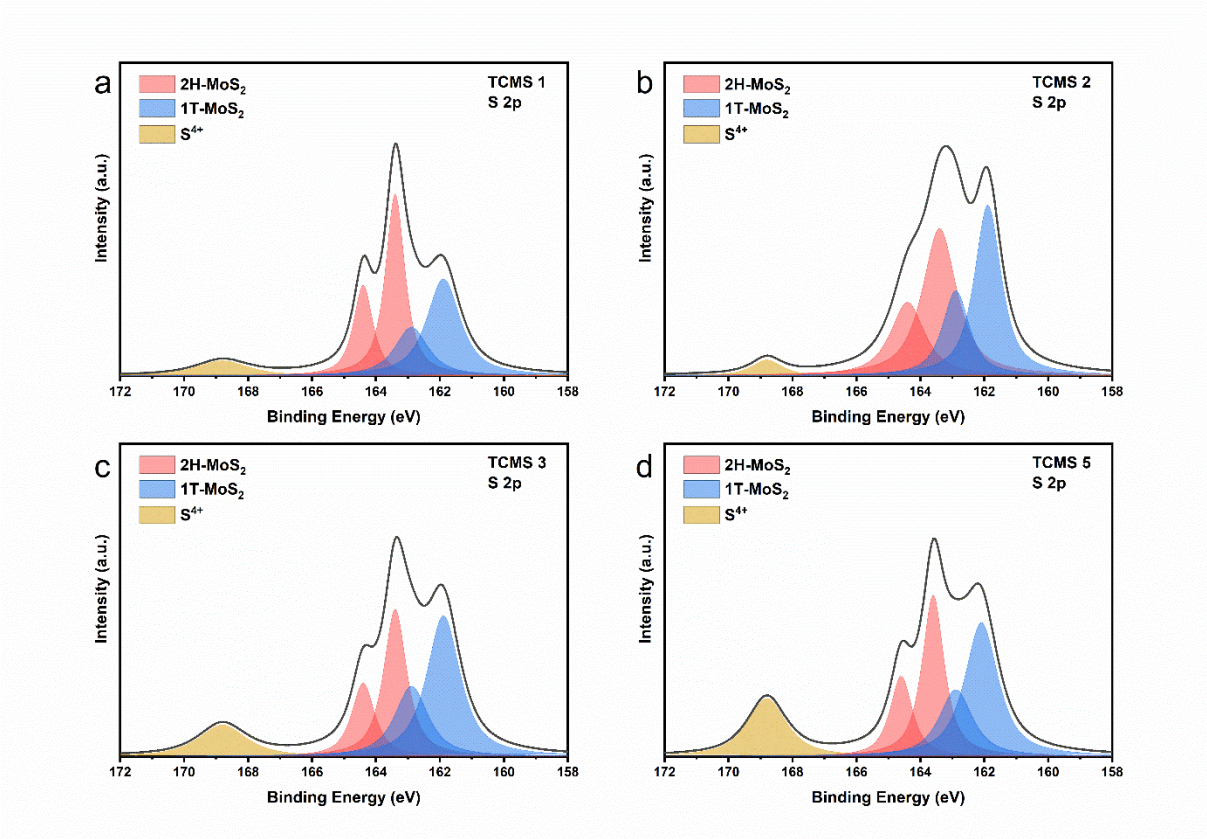

Figure S6. High-resolution XPS spectra of the S 2p peak region of (a) TCMS 1, (b) TCMS 2, (c) TCMS 3, and (d) TCMS 5.

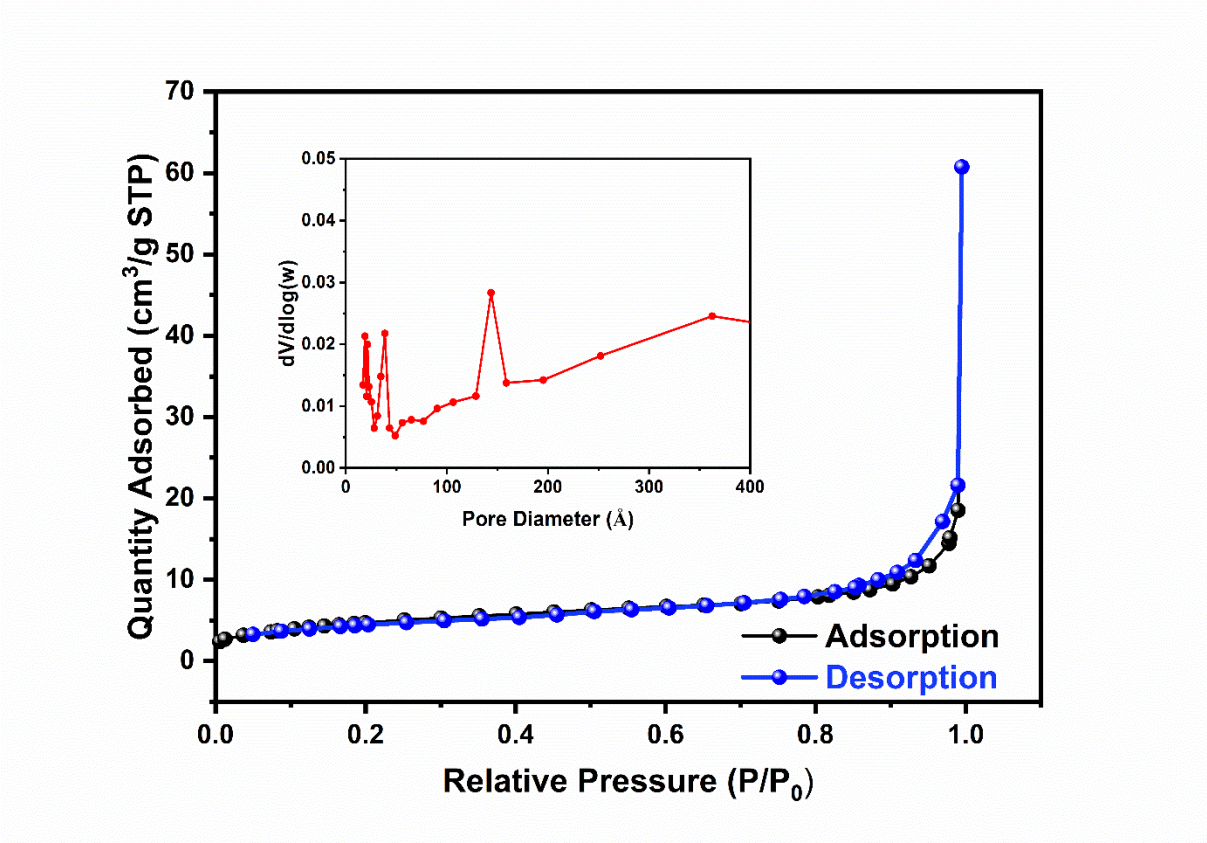

Figure S7. N_2 adsorption-desorption isotherms from BET measurements and (in the inset) the pore-size distribution for TCMS 4.

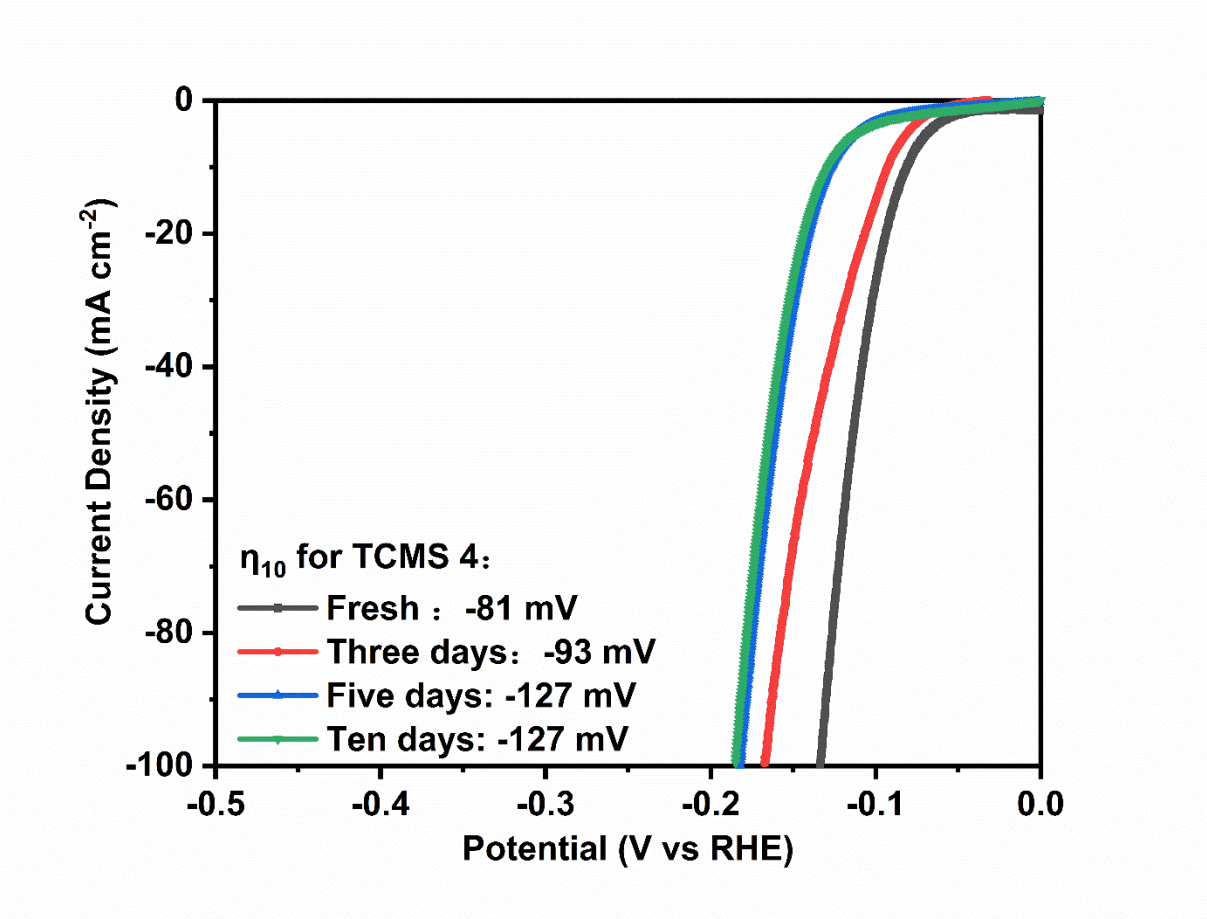

Figure S8. Linear sweep voltammetry curves (scan rate 1 $mV \cdot s^{-1}$) of TCMS 4 electrodes tested in 0.5 M H_2SO_4, which were fresh and stored (in air) for 3, 5, and 10 days.

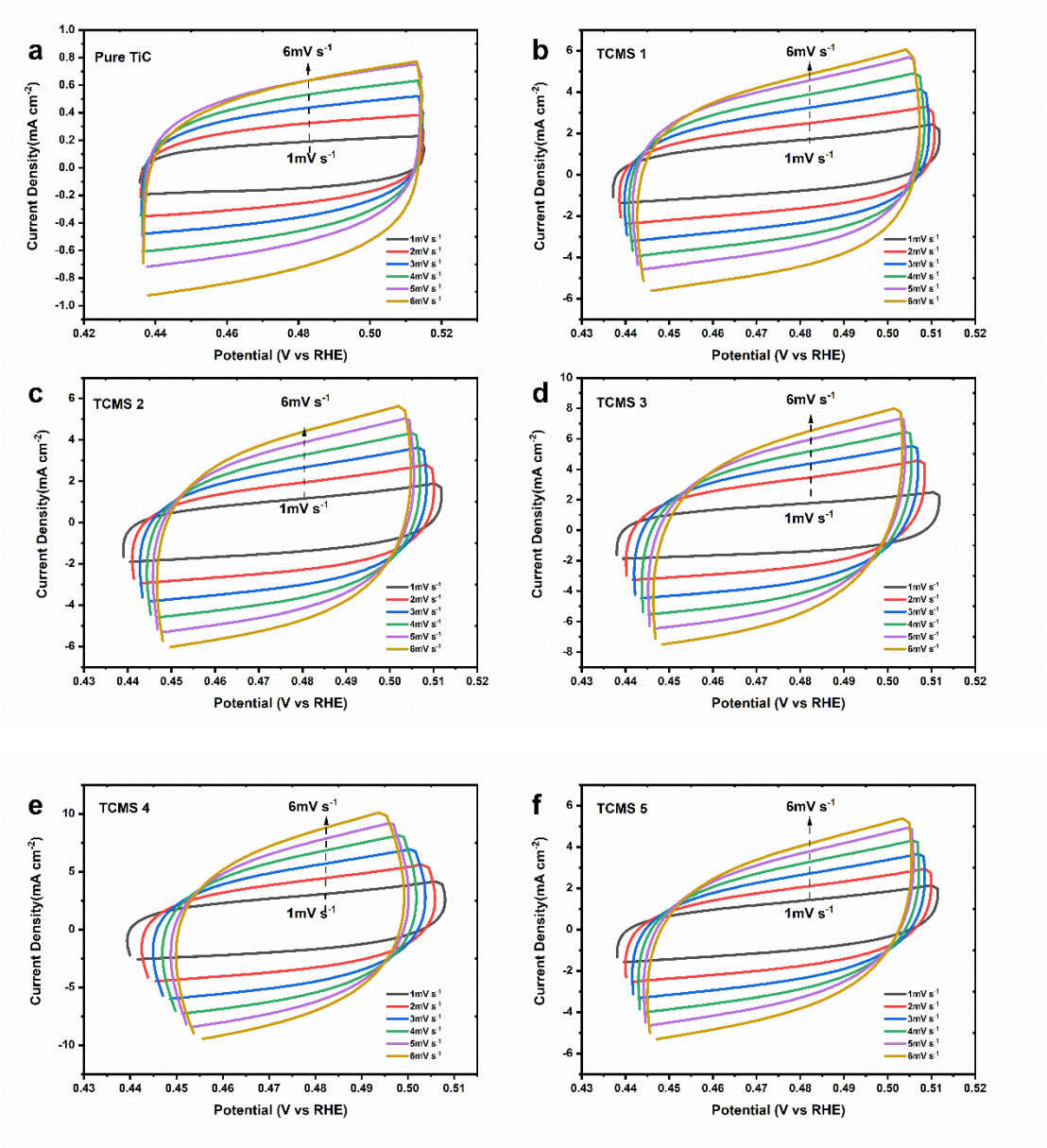

Figure S9. Cyclic voltammogram curves of (a) TiC, (b) TCMS 1, (c) TCMS 2, (d) TCMS 3, (e) TCMS 4, and (f) TCMS 5 in the double layer capacitive region at the scan rates from 1 to 6 $mV \cdot s^{-1}$.

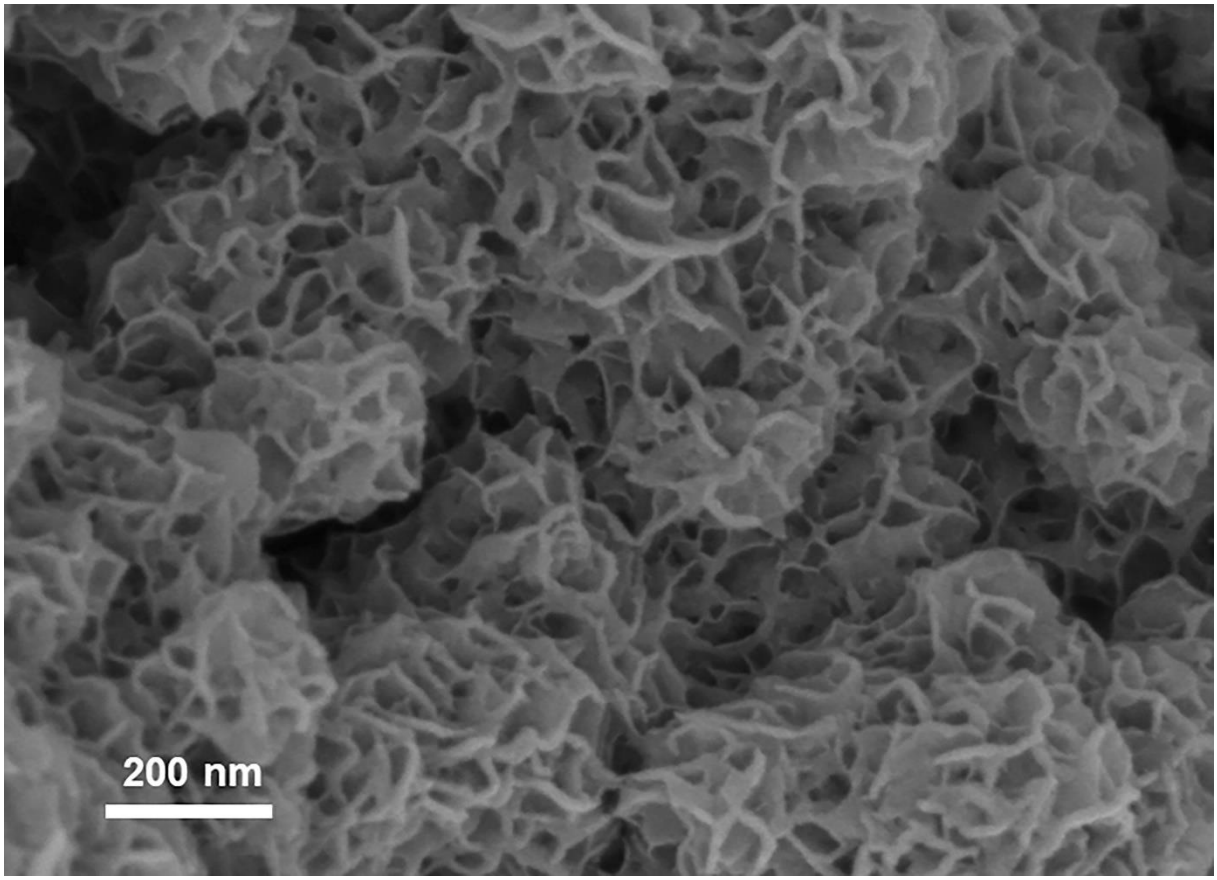

Figure S10. SEM image of MoS_2 layer of TCMS 4 after 5000 cycles of CV testing.

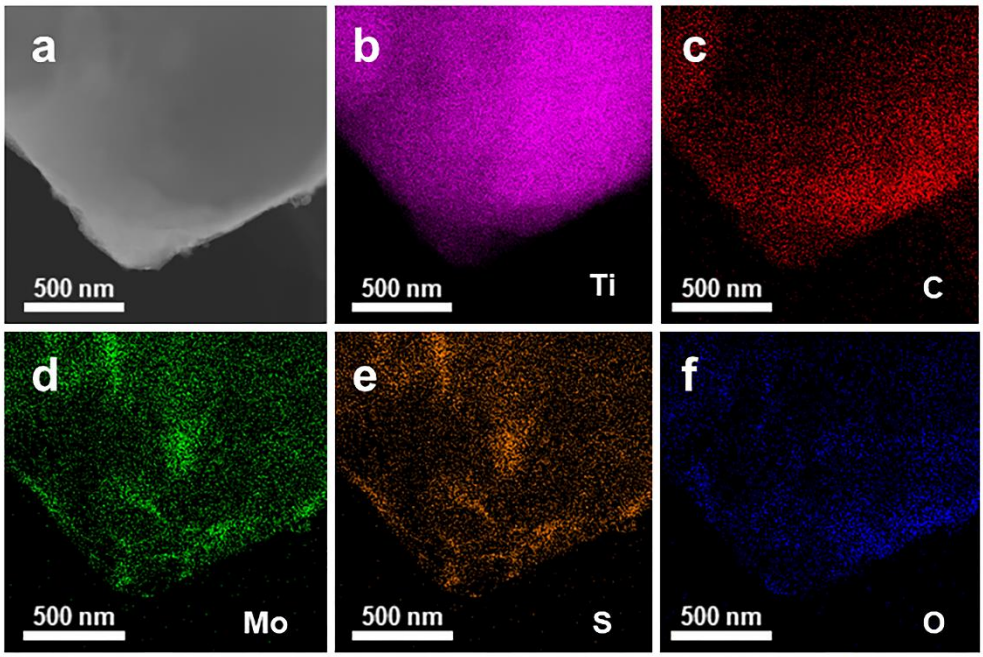

Figure S11. (a) Morphology and (b-f) EDS elemental mapping of TCMS 4 after HER test.

Table S1. Comparison of the parameters of HER performance reported in this study and in other studies on MoS_2-based catalysts supported on various substrates.

Catalysts	Synthesis technique	η_{10} [mV]	Tafel slope [mV dec^{-1}]	Rct [Ω]	Stability (CV tests or i-t time)	C_{dl} [mF cm^{-2}]	Ref.
TCMS 4	Hydrothermal	-127	41	13.4	24 h+ 5000 cycles	1079.4	This study
MoS_2/ MoO_2 on reduced graphene oxides foam loaded on a glassy carbon electrode by binders	Chemical vapor deposition	-197	215	/	2000 cycles	79.6	[4]
MoS_2 nanoplates embedded in Co-N-doped nanocage loaded on a glassy carbon electrode by binders	Template	-180	74	130	1000 cycles	21.07	[5]
Vertically grown MoS_2 nanoplates on vanadium nitride loaded on a glassy carbon electrode by binders	Hydrothermal	-85	53.31	467	1000 cycles	/	[6]
MoS_2 nanosheets grown on synthesized Bi_2Se_3 nanoflowers loaded on a glass carbon electrode by binders	Hot injection method	-208	57	53.4	1000 cycles	1.73	[7]
Nitrogen-doped MoS_2 anchored on a porous carbon network loaded on a glass carbon electrode by binders	Annealing method	-114	46.8	6	1000 cycles	26.93	[8]
CuS@ defect-rich MoS_2 core-shell structure dispersed on a glassy carbon electrode by binders	Hydrothermal	-135	50	20	3000 cycles	22.80	[9]
Wafer-scale sulfur vacancy-rich monolayer MoS_2 on glassy carbon by binders	Laser molecular beam epitaxy	-256	93	90	10000 cycles	11.44	[10]
Core-shell CoS_2 @MoS_2 nanoparticles coated on a glassy carbon electrode by binders	Hydrothermal	-276	60	750	1000 cycles	2.79	[11]
P-doped MoS_2 on N, S-doped reduced graphene oxide drop cast on a glassy-carbon rotating disk	Hydrothermal	-94	47	40	20 h	/	[12]

electrode by binders							
RuO_2@ MoS_2 drop cast on a glassy carbon electrode by binders	Hydrothermal	-114	62.9	102	2000 cycles	8.7	[13]
1T-MoS_2 on carbon cloth drop cast on a glassy carbon electrode by binders	Hydrothermal	-151	55	25	5000 cycles	125.6	[14]
(Ni, Fe) S_2@MoS_2 heterostructures grown on carbon fiber paper as an electrode	Hydrothermal	-130	101.22	3	44 h	0.67	[15]
3D flower-like defected MoS_2 on candle soot substrate loaded on a glassy carbon electrode by binders	Magnetron-sputtered	-56	49	3	46 h	52.39	[16]
MoS_2 on semimetal $CoMoP_2$ directly as an electrode	Electrochemical	-75	109	/	40 h+ 5000 cycles	412	[17]
Phosphorus-doped MoS_2 on the glassy carbon loaded on a glassy carbon electrode by binders	Post-doping method	-215	52	294	1000 cycles	8.92	[18]
3D edge rich MoS_2 directly grown on the glassy carbon as an electrode	Chemical vapor deposition Oxygen plasma etching	-297	207	/	1000 cycles	/	[19]
$NiCo_2O_4$@MoS_2 directly grown on the carbon paper	Hydrothermal	-180	79.4	4.74	20 h	/	[20]

References

(1) NIST X-ray Photoelectron Spectroscopy Database, NIST Standard Reference Database Number 20 (National Institute of Standards and Technology, Gaithersburg MD). **2000**.

(2) Shard, A. G., Practical guides for x-ray photoelectron spectroscopy: Quantitative XPS. *J. Vac. Sci. Technol. A.* **2020**, *38*, 041201.

(3) Deng, J.; Li, H.; Wang, S.; Ding, D.; Chen, M.; Liu, C.; Tian, Z.; Novoselov, K. S.; Ma, C.; Deng, D.; Bao, X., Multiscale structural and electronic control of molybdenum disulfide foam for highly efficient hydrogen production. *Nat. Commun.* **2017**, *8*, 14430.

(4) Joyner, J.; Oliveira, E. F.; Yamaguchi, H.; Kato, K.; Vinod, S.; Galvao, D. S.;Salpekar, D.; Roy, S.; Martinez, U.; Tiwary, C. S.; Ozden, S.; Ajayan, P. M. Graphene Supported MoS_2 Structures with High Defect Density for an Efficient HER Electrocatalysts. *ACS Appl. Mater. Interfaces* **2020**, *12*, 12629-12638.

(5) Hou, X.; Zhou, H.; Zhao, M.; Cai, Y.; Wei, Q. MoS_2 Nanoplates Embedded in Co–N-Doped Carbon Nanocages as Efficient Catalyst for HER and OER. *ACS Sustain. Chem. Eng.* **2020**, *8*, 5724-5733.

(6) Meng, K.; Wen, S.; Liu, L.; Jia, Z.; Wang, Y.; Shao, Z.; Qi, T. Vertically Grown MoS_2 Nanoplates on VN with an Enlarged Surface Area as an Efficient and Stable Electrocatalyst for HER. *ACS Appl. Energy Mater.* **2019**, *2*, 2854-2861.

(7) Li, D.; Lao, J.; Jiang, C.; Shen, Y.; Luo, C.; Qi, R.; Lin, H.; Huang, R.; Waterhouse, G. I. N.; Peng, H. Heterostructured MoS_2@Bi_2Se_3 nanoflowers: A highly efficient electrocatalyst for hydrogen evolution. *J. Catal.* **2020**, *381*, 590-598.

(8) Hao, W.; Xu, X.; Shuyuan, L.; Chao-Lung, C.; Xiaoxiao, K.; Chun-Kuo, P.; Yu-Chang, L.; Xing, M.; Jianqing, Z.; Jinho, C.; Yan-Gu, L.; Jong-Min, L.; Lijun, G. Structural and Electronic Optimization of MoS_2 Edges for Hydrogen Evolution. *J. Am. Chem. Soc.* **2019**, *141*, 18578-18584.

(9) Liu, L.; Liu, X.; Jiao, S. CuS@defect-rich MoS_2 core-shell structure for enhanced hydrogen evolution. *J. Colloid Interface Sci.* **2020**, *564*, 77-87.

(10) Hu, C.; Jiang, Z.; Zhou, W.; Guo, M.; Yu, T.; Luo, X.; Yuan, C. Wafer-Scale Sulfur Vacancy-Rich Monolayer MoS_2 for Massive Hydrogen Production. *J. Phys. Chem. Lett.* **2019**, *10*, 4763-4768.

(11) Wei, Q.; Ye, Z.; Ren, X.; Li, X.; Yin, M.; Zan, L.; Fu, F. Core-shell CoS_2@MoS_2 nanoparticles as an efficient electrocatalyst for hydrogen evolution reaction. *J. Alloy. Compd.* **2020**, *835*, 155264.

(12) Guruprasad, K.; Maiyalagan, T.; Shanmugam, S. Phosphorus Doped MoS_2 Nanosheet Promoted with Nitrogen, Sulfur Dual Doped Reduced Graphene Oxide as an Effective Electrocatalyst for Hydrogen Evolution Reaction. *ACS Appl. Energy Mater.* **2019**, *2*, 6184-6194.

(13) Liu, Z.; Jiang, J.; Liu, Y.; Huang, G.; Yuan, S.; Li, X.; Li, N. Boosted hydrogen evolution reaction based on synergistic effect of RuO_2@MoS_2 hybrid electrocatalyst. *Appl. Surf. Sci.* **2021**, *538*, 148019.

(14) Zhipeng, L.; Lei, Z.; Yuhua, L.; Zhichao, G.; Shisheng, Y.; Xiaotian, L.; Nan, L.; Shiding, M. Vertical nanosheet array of 1T phase MoS_2 for efficient and stable hydrogen evolution. *Appl. Catal. B.* **2019**, 246, 296-302.

(15) Liu, Y.; Jiang, S.; Li, S.; Zhou, L.; Li, Z.; Li, J.; Shao, M. Interface engineering of (Ni, Fe)S_2@MoS_2 heterostructures for synergetic electrochemical water splitting. *Appl. Catal. B.* **2019**, *247*, 107-114.

(16) Gao, B.; Du, X.; Ma, Y.; Li, Y.; Li, Y.; Ding, S.; Song, Z.; Xiao, C. 3D flower-like defected MoS_2 magnetron-sputtered on candle soot for enhanced hydrogen evolution reaction. *Appl. Catal. B.* **2020**, *263*, 117750.

(17) Li, G.; Fu, C.; Wu, J.; Rao, J.; Liou, S.-C.; Xu, X.; Shao, B.; Liu, K.; Liu, E.; Kumar, N.; Liu, X.; Fahlman, M.; Gooth, J.; Auffermann, G.; Sun, Y.; Felser, C.; Zhang, B. Synergistically creating sulfur vacancies in semimetal-supported amorphous MoS_2 for efficient hydrogen evolution. *Appl. Catal. B.* **2019**, *254*, 1-6.

(18) Ren, X.; Yang, F.; Chen, R.; Ren, P.; Wang, Y. Improvement of HER activity for MoS_2: insight into the

effect and mechanism of phosphorus post-doping. *New J. Chem.* **2020**, *44*, 1493-1499.
(19) Li, S.; Zhou, S.; Wang, X.; Tang, P.; Pasta, M.; Warner, J. H. Increasing the electrochemical activity of basal plane sites in porous 3D edge rich MoS_2 thin films for the hydrogen evolution reaction. *Mater. Today Energy* **2019**, *13*, 134-144.
(20) Li, J.; Chu, D.; Baker, D. R.; Dong, H.; Jiang, R.; Tran, D. T. Distorted Inverse Spinel Nickel Cobaltite Grown on a MoS_2 Plate for Significantly Improved Water Splitting Activity. *Chem. Mater.* **2019**, *31*, 7590-7600.